Investigation of fatigue cracking in aluminium 7075 alloys and the role of heat treatment

Robert Rutto, Cleophas Obara & Shagwira Harrison

Check for updates

Investigation of fatigue cracking in aluminium 7075 alloys and the role of heat treatment

Robert Rutto, Cleophas Obara and Shagwira Harrison [iD]

Department of Mechanical Engineering, Moi University, Eldoret, Kenya; Department of Mechanical Engineering, Dedan Kimathi University of Technology, Nyeri, Kenya; Department of Mechanical and Industrial Engineering, Masinde Muliro University of Science and Technology, Kakamega, Kenya

ABSTRACT

The unique properties of aluminium alloys and their high strength-to-weight ratio make them the preferred choice for aircraft design. However, fatigue cracking in ageing fleets remains significant. This study investigates microstructural cracking of cooled and heat-treated Al 7075–0, T6, and T7 alloys used in airframes and stringers. To study the effect of heat treatment, medium voltage test pieces were used according to the guidelines of ASTM E647. Scanning Electron Microscopy (SEM) was used to observe the crack surface morphology. The results show that Al 7075-T7 exhibits higher resistance to the Fatigue crack growth (FCG) threshold than Al 7075-O and T6. In the case of the quenched Al 7075-O, the fatigue performance remains constant for samples oriented with a perpendicular and countersunk rivet hole. SEM analysis of fatigue cracking surface indicates that the microcracks leading to fracture originate from inclusion zones, secondary stage grains, and micro-structural defects. In addition, as the heat treatment condition increased from O to T6 to T7, the area of the semi-subdivision planes and the width of the fatigue bands initially increased and then decreased. The final fault zones exhibit dimpled properties, with increasing size and deeper changing depth as heat treatment annealing progresses from O to T6 to T7. In summary, the study highlights the outstanding fatigue resistance of Al 7075-T7 and provides valuable insights into the microstructural aspects of fatigue cracking in aircraft alloys subjected to different heat treatments. These results contribute to the understanding and managing of ageing fleets, supporting the development of more reliable aircraft designs.

1. Introduction

The unique properties of aluminium alloys and their strength-to-weight ratio make them the preferred choice for designing aircraft with better design safety margins and improved payload [1–3]. Massive resistance to the propagation of fatigue cracks and enhanced formability of the alloys reduce manufacturing costs and process flow time. Alloy 7075-T6 is used where compressive strength is a critical design

principle, for example, in aircraft stringers and frames [4]. During maintenance, several aircraft operators report cracking failure of parts made of aluminium alloy 7075-T6, specifically the frames and stringers [4, 5]. The remedy is to repair or replace the parts, which takes at least 5 days of lost revenue. A compromised structural member carrying primary and secondary loads makes operating an aircraft unsafe. According to the Boeing Multi Operator Message MOM-MOM-19-0536-01B, eighteen aeroplanes were inspected, including 737–700 and 737–800 variants. Of the eighteen, three cracks were reported. One aircraft showed cracks on its left and right frame fitting's outer chords, and another showed a crack on the right frame fitting outer chord [6]. The cracks observed can be attributed to repetitive loading experienced on aircraft structures during flight cycles, causing fatigue failure over time. The high-stressed regions, such as frame fittings, may experience crack initiation and propagation due to the cumulative stress cycles. Additionally, the operational circumstances of the aircraft, including takeoff, landing, and manoeuvring, subject the frame fittings to different types of loads that may cause crack formation [7].

Studies on the influence of notch geometry and mean stress on fatigue life initiation on Al alloy 7075 T6 and 7075 T71 have been performed by Benachour *et al.* [8] while applying constant amplitude loading and a local strain approach. The results confirmed that fatigue life is related to crack initiation. After the initial heat treatment (solution heat treatment), the alloy 7075 T6 is then rapidly quenched to room temperature, which results in the alloy reaching a stable condition known as the T6 temper. The 'T' stands for 'thermally treated' [9]. The aluminium alloy 7075 possesses excellent mechanical properties and high strength, making it suitable for various aerospace and structural applications. In the T71 condition, the aluminium alloy 7075 is over-aged, which means it is subjected to an extended ageing process compared to the T6 temper. This over-ageing results in the alloy maintaining its strength levels very close to the conventional T6 temper while achieving improved stress corrosion resistance [10]. Fakioglu *et al.* [11] determined the fatigue behaviour and fracture characteristics of the Al 7075 alloys aged through different methods.

The effect of the precipitates formed in the matrix through ageing depended on the damage tolerance of the heat treatment process. Gačo *et al.* [12] studied the effects of heat treatment temperatures of 420°C, 460°C, and 500°C on fatigue life and fatigue strength on an aluminium alloy substrate. The study noted an improvement in fatigue initiation and propagation life of aluminium alloy specimens heat-treated at higher temperatures than those heat-treated at low temperatures. The value of fatigue strength for newly formed material at room temperature was 79% of yield stress. The yield stress for new material was 65% at 545°C. Permanent fatigue strength measured at maximum operating temperature was 64% yield stress. As a result of the more efficient dissolution and precipitation reactions at higher heat treatment temperatures, the aluminium alloy's microstructure is filled with finely dispersed, stable precipitates. When cyclic stress, a component of fatigue loading, occurs, these precipitates act as barriers to dislocation movement inside the material. The development of precipitates increases the material's resistance to fatigue crack initiation and propagation, extending the fatigue life. The input process parameters identified in the literature include: thermo-mechanical processing [13], ageing treatment [14,15], stress ratio [16,17] and riveting parameters [18].

Even though aluminium alloys, particularly 7075-T6, are preferred for aircraft design because of their strength-to-weight ratio and affordability, some operators have observed cracking failures in crucial components like frames and stringers. To improve the understanding of fatigue cracking and guarantee long-term aircraft safety and performance, thorough tests and cooperative efforts are required between manufacturers, operators, and researchers. This study focused on the effects of microstructure, nature of grains, rivet-hole geometry and heat treatment on the fatigue performance of aluminium alloys 7075–0/T6/T7 through fatigue loading tests and micro-structural analysis.

2. Methodology

In this study, 7075 aluminium alloy, equivalent to the material used in aircraft frames and stringers, was procured as 7075-O and 7075-T6. Al 7075-T6 was converted to Al 7075-T7 by heating it as per Boeing standard BAC562. The middle tension [M(T)] specimen was utilised as the standard test method for crack growth rates as per ASTM E647 [19]. Three samples were used per experiment. The specimens designed for crack initiation at different rivet hole orientations were prepared as per ASTM E8 [20] to avoid cracking at the gripping holes. Figure 1 shows some of hole geometries that are used in the study of crack initiation.

High-cycle fatigue testing (Constant-Force-Amplitude Test Procedure) on the specimens was performed at the University of Nairobi, Department of Mechanical Engineering workshop. Dummy tests were conducted before the actual test for each specimen with an R ratio of 0.33, P_{min} = 90 lbs (400.34N), P_{max} = 270 lbs (1201.01N), and load frequency of 1498 Hz. The R ratio is a crucial variable in fatigue testing because it influences the stress state that the material experiences during the cyclic loading. In each cycle of the test, it establishes the loading parameters and stress range that the material will experience. With an R ratio of 0.33, the test simulates the actual loading conditions and offers more relevant information for engineering applications [21,22].

The equipment setup for fatigue testing was done, ensuring that the force distribution was symmetrical to the specimen notch. A stopwatch was used to determine the elapsed time in minutes for each crack advancement, which aided in determining the elapsed cycles. To reduce the time taken experimenting, the load frequency chosen for testing fatigue and crack proliferation was slightly more than that experienced in service conditions or real-life scenarios. A travelling microscope was used to measure the crack length. The data for fatigue crack advancement rate (da/dN) calculated experimentally
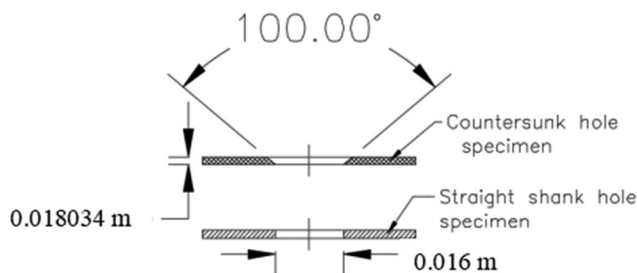

Figure 1. Hole geometries of specimens designed for the study of crack initiation.

against the range of stress intensity factor (ΔK) was generated via incremental technique. The experimental data were correlated using the Paris law.

$$\frac{da}{dN} = C\Delta K^m \tag{1}$$

represented in a plot of Log-log (da/dN) against ΔK for all materials as indicated in the form of

$$Log\left(\frac{da}{dN}\right) = logC + mlog(\Delta K) \tag{2}$$

Where C and m are material constants.

The cracked surfaces were cut into four pieces; (i) CI-Crack Initiation (6 mm length), (ii) CPS-slow crack propagation (6 mm length), (iii) CPF-fast crack propagation (6 mm length), and (iv) FF-final fatigue fracture (6 mm length). The standardised crack length of 6 mm for each section of the cracked surface allowed for consistent and repeatable measurements and analysis. It was decided by considering factors such as having a good sample size that can optimally portray the characteristic features under study [11].

Figure 2 shows the fatigue crack growth (FCG) rate. This particular graph has ΔK on the x-axis and da/dN on the y-axis, representing the crack's magnitude and the total number of cycles leading to failure, respectively. There are three distinct portions in this graph. In Regime A, the crack propagation rate rapidly declines as ΔK is reduced. It is significant to note that fracture growth can happen below K_{th}, even if fatigue damage is unlikely to occur at that level. In a log plot, the fracture growth rate in regime B is linear.
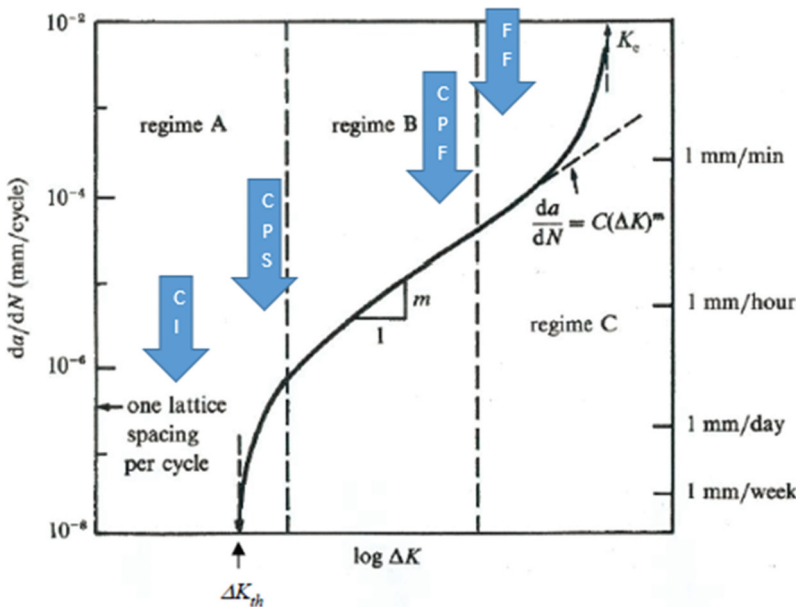

Figure 2. Fatigue crack growth (FCG) curve showing the crack growth derivative (da/dN) vs log ΔK describing the three regions (regimes A, B and C) associated with crack growth rate, K_{th} is the threshold intensity range while K_c is the fracture toughness [23].

It adheres to Paris' law, which is expressed by Eq. (1), where ΔK is the stress intensity factor ranging from (K_{max} - K_{min}), C, and m are experimental constants, and where the environment, temperature, material variables, frequency, and stress ratio are dependent on the values of these variables [24]. The other regime involves accelerated crack growth. SIF grows to the maximum value in the cycle, i.e. Kmax reaches the fracture toughness (K_C), which depends on the material environment, strain rate, temperature, and specimen geometry [25]. This occurs after the typical linear stable macroscope crack growth [26].

Then, etching was done using Keller's reagent to show the microstructure of metals and alloys. Etching the specimens allows scientists to notice grain boundaries, precipitates, and other microstructural components. This enables them to investigate how the microstructure affects crack propagation behaviour and fatigue performance [26]. The crack surface morphology was observed by a standard scanning electron microscope (with an acceleration voltage of 20 kV at Busitema University, Uganda).

3. Results and discussion

3.1. Effect of heat treatment on heat treatment conditions

The impacts of heat treatment on crack growth and propagation under constant fatigue loading of Al alloy 7075 under varied heat treatment conditions (-O, -T6, -T7) were studied in a fatigue testing machine. The superimposed propagation curves da/dN against ΔK are illustrated in Figure 3 for the three heat-treated conditions Al alloys 7075-
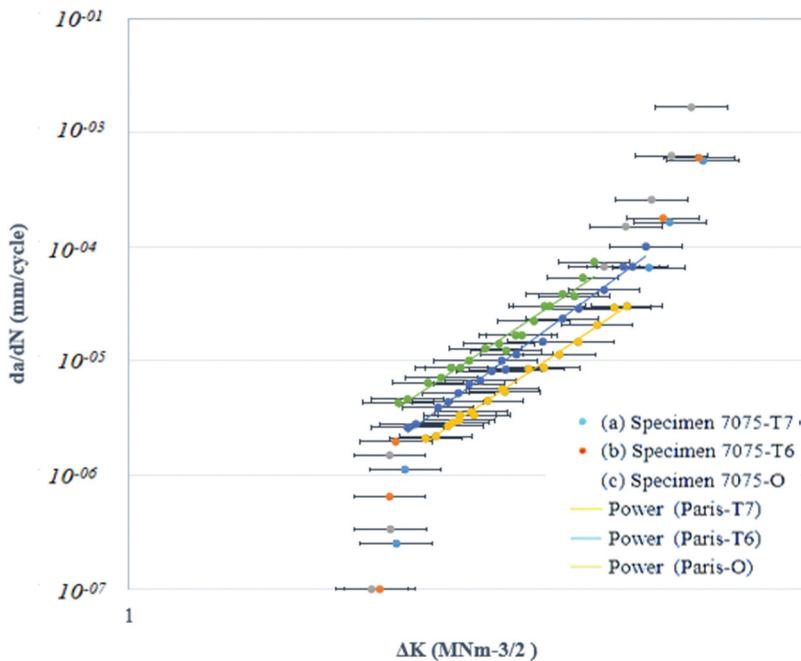

Figure 3. Superimposed fatigue crack growth curves for Al 7075-O, T6 and T7 with their respective power Paris lines at a constant amplitude of ΔP =1201 N, R = 0.33.

T7, T6 and O for R = 0.33, as seen from the graphs of the results. The Al alloys 7075-T7 condition demonstrated a more prominent resistance against crack propagation than the Al alloys 7075-O condition.

The curves concur with those acquired by Leng *et al.* [23]. In the study, compared to alloy 7075-O, alloy 7075-T7 demonstrated even stronger resistance to crack propagation under slow crack growth conditions. The difference in fracture resistance between the two states increased when the crack growth rates decreased and got closer to a critical threshold value. Al alloys 7075-T6 condition displays an intermediate behaviour between Al alloys 7075-O and Al alloys 7075-T7 and grows towards Al alloys 7075-T7 above 10^{-3} mm/cycle. The behaviour of solution-heated, artificially aged aluminium alloy 7075-T6 falls between alloys 7075-O and 7075-T7. The 'intermediate behaviour' indicates that it has a stronger fracture propagation resistance than the fully annealed (7075-O), but not as high as that of overaged (7075-T7). This was expected since the T6 temper balances mechanical qualities acquired during ageing. The da/dN is greater while ΔK_{th} is less for the Al alloys 7075-O state than for the Al alloys 7075-T7 one while Al alloys 7075-T6 is sandwiched among the two. The monitored greater da/dN and less ΔK_{th} under the Al alloys 7075-O condition than under the Al alloys 7075-T7 and 7075-T6 states are also registered by other researchers [20, 27, 28].

The crack propagation curves of the Al alloys 7075-O, 7075-T6 and 7075-T7 are represented for $R = 0.33$ by straight lines along the Paris region, i.e. the Power equation for Paris region for the three heat treatment conditions gives;

Al alloys 7075-T7 gives, y = 3×10^{-7} x $(\Delta K)^{10.069}$
Al alloys 7075-T6 gives, y = 4×10^{-7} x $(\Delta K)^{10.069}$
Al alloys 7075-O gives y = 1×10^{-6} x $(\Delta K)^{9.663}$
Representing the same on Paris equation 1 gives, for Al alloys of:
7075-T7 it becomes

$$\left(\frac{da}{dN}\right) = 3x10 - 7(\Delta K)^{10.069}$$

7075-T6 it becomes

$$\left(\frac{da}{dN}\right) = 4x10^{-7}(\Delta K)^{10.869}$$

7075-O becomes

$$\left(\frac{da}{dN}\right) = 1x10^{-6}(\Delta K)^{9.663}$$

Assuming the stress intensity factor is constant, for this case, let us take $\Delta K = 2$
For Al alloys 7075-T7

$$\left(\frac{da}{dN}\right) = 3x10^{-07}(2)^{10.869}$$

$\left(\frac{da}{dN}\right)_{7075-T7} = 3.22x10^{-4}$ mm/cycle

For Al alloys 7075-T6

$$\left(\frac{da}{dN}\right) = 4\text{x}10^{-07}(2)^{10.869}$$

$$\left(\tfrac{da}{dN}\right)_{7075-T6} = 7.48\text{x}10^{-4} \text{ mm/cycle}$$

For Al alloys 7075-O

$$\left(\frac{da}{dN}\right) = 1\text{x}10^{-06}(2)^{10.869}$$

$$\left(\tfrac{da}{dN}\right)_{7075-O} = 8.10\text{x}10^{-4} \text{ mm/cycle}$$

The exact value of ΔK, the crack propagation rate of Al alloys 7075-T7 is consistently inferior to the crack propagation rate of Al alloys 7075-T6 and 7075-O, and they tend to become identical beyond $1\text{x}10^{-3}$ mm/cycle. We again witness that, in this model, it is inconceivable to determine a point as an asymptotic boundary of the crack propagation curves.

Determining ΔK_{th} for different heat treatment materials.

For Al alloys 7075-T7 becomes

$$\left(\frac{da}{dN}\right) = 3\text{x}10^{-07}(\Delta K)^{10.069}$$

$$10^{-7} = 3\text{x}10^{-07}(\Delta K)^{10.069}$$

$$\Delta K_{th} = 0.8966$$

For Al alloys 7075-T6 becomes

$$\left(\frac{da}{dN}\right) = 4\text{x}10^{-07}(\Delta K)^{10.869}$$

$$10^{-7} = 4\text{x}10^{-07}(\Delta K)^{10.869}$$

$$\Delta K_{th} = 0.8802$$

For Al alloys 7075-O becomes

$$\left(\frac{da}{dN}\right) = 1\text{x}10^{-06}(\Delta K)^{9.663}$$

$$10^{-7} = 1\text{x}10^{-06}(\Delta K)^{9.663}$$

$$\Delta K_{th} = 0.7880$$

The interpretation of fatigue crack propagation rates da/dN against stress intensity span ΔK for Al alloys 7075-O, 7075-T6 and 7075-T7 conditions is shown in Figure 4, for load ratio 0.33, constant amplitude. Close to threshold levels, it is apparent that Al alloy 7075-T7 structures offer the most elevated fatigue resistance in spans of the most inferior growth rates and the highest threshold point ΔK_{th} values. Likened with those for the Al alloy 7075-O configuration, the threshold
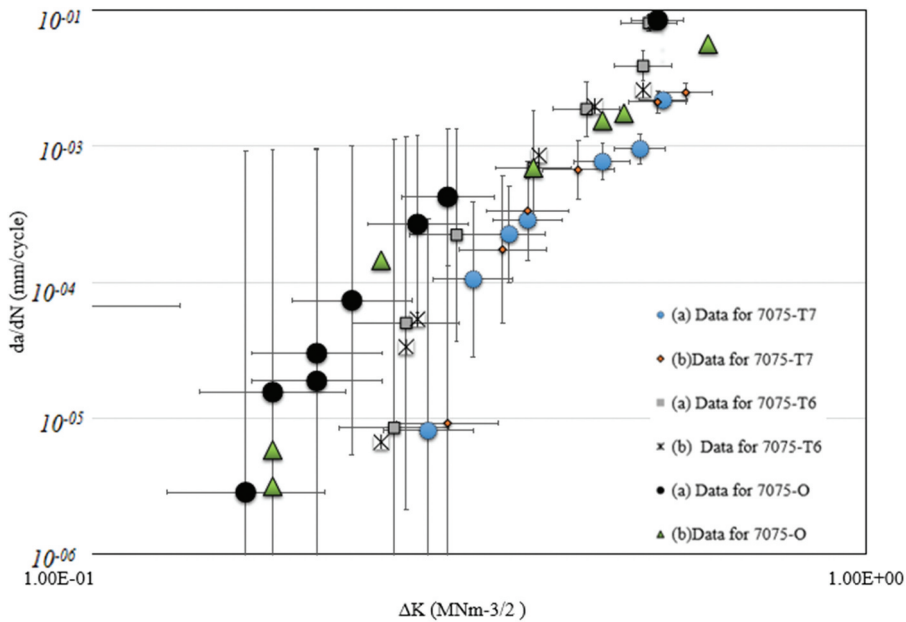
Figure 4. Superimposed fatigue crack growth of Al 7075-O/T6/T7 at a constant amplitude of $\Delta P = 1201$ N, $R = 0.33$ with (a) countersunk 100 rivet hole and (b) perpendicular rivet hole orientation.

Table 1. Material parameters.

Al alloys 7075 material condition	c	m	ΔK_{th} (MNm$^{-3/2}$)	da/dN (assumption, $\Delta K = 2$) mm/cycle
7075-T7	3×10^{-07}	10.069	0.8966	3.22×10^{-4}
7075-T6	4×10^{-07}	10.869	0.8802	7.48×10^{-4}
7075-O	1×10^{-06}	9.663	0.7880	8.10×10^{-4}

ΔK_{th} values in the current developments are approximately 11% and 14% more heightened in the Al alloy 7075-T6 and 7075-T7 configurations, respectively, ΔK_{th} standard deviation is 0.0478, at $R = 0.33$ as shown in Table 1.

3.2. Effect of rivet hole orientation

The determination of crack propagation under constant fatigue loading in a 100° countersunk rivet hole and straight rivet hole geometry of Al 7075-O, Al 7075-T6, and Al 7075-T7 alloy specimens was investigated through a fatigue testing machine. The superimposed fatigue crack growth graph for Al alloy 7075-O, 7075-T6, and 7075-T7 is depicted in Figure 4, showing the fatigue growth of countersunk and perpendicular rivet hole geometry.

Based on the data presented in Figure 4, the rivet hole geometry has a negligible impact on the fatigue lives of the countersunk and perpendicular rivet hole for Al alloy 7075-O, 7075-T6, and 7075-T7. The superimposed fatigue crack growth graph for Al alloy 7075-O is depicted in Figure 4, showing the fatigue growth of the

countersunk following the curve for perpendicular rivet hole orientation for the respective heat treatment conditions 7075-O, 7075-T6, and 7075-T7. The hole geometry did not affect the fatigue crack growth rate for Al alloy 7075-T7. Its superimposed graph depicted the growth graph of countersunk and perpendicular are in line with each other.

A superimposed graph of all the three heat-treated conditions with different hole geometry showed that Al alloy 7075-T7 has higher and lower ΔK_{th} than Al alloy 7075-T6 and Al alloy 7075-O. Al alloy 7075-T6 is the bandwidth between Al alloy 7075-T7 and Al alloy 7075-T6, which agrees with the results found and other scholars [29, 30]. In summary, the specimen geometry used to study hole geometry did not provide enough data to determine the Paris region.

3.3. Fatigue fractographic analysis

The typical crack paths in the Al alloy 7075-O, 7075-T6 and 7075-T7 specimens are shown in Figure 5. In the Al Alloy 7075-O sample, the crack path associated with fatigue is sharply angled and twisting, deflecting, and branching, as shown in Figure 5(a), and measured deflection angles through the optical microscope are about 30°, 45°, and 70°, with a standard deviation of 17. Al alloy 7075-T6 and 7075-T7 samples exhibit nearly straight, linear, with no deflection fatigue crack path as depicted in Figures 5(b,c). The failure analysis for the fracture surface is trans-granular in all subjects with proof of slip steps, facets and ledges. Such facets are mainly enunciated in the Al alloy 7075-O form and have an appearance aspect of crystallographic fatigue surfaces [23,30,31]. In distinction with Al alloy, 7075–0 fractures displaying a zigzag appearance, Al alloy 7075-T6 and 7075-T7 are predominately linear, outlying fewer crack deflections crack paths.
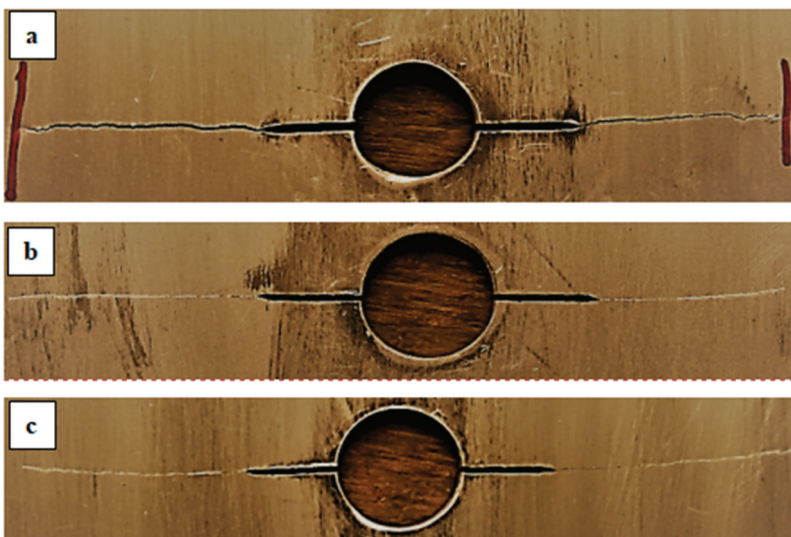

Figure 5. (a) Crack path for Al 7075-O, (b) crack path for Al 7075-T6, (c) crack path for Al 7075-T7.

3.4. Fatigue fracture morphology observation of al alloy 7075-O/T6/T7

3.4.1. Fatigue crack initiation

From this study, the fatigue-fractured surface morphology of the fatigue initiation of Al alloys (a) 7075-O, (b) 7075-T6, and (c) 7075-T7 were examined, as indicated in Figure 6.

The fatigue fracture surfaces of tests Al alloy 7075-O, 7075-T6 and 7075-T7 under $R = 0.33$ were examined in scanning electron microscopy (SEM). Figure 6 illustrates the all-around fracture surfaces and the fatigue crack initiation for (a) 7075-O, (b) 7075-T6, and (c) 7075-T7. The failure analysis for the fracture surfaces consists of fatigue crack initiation regions for the three heat-treated conditions.
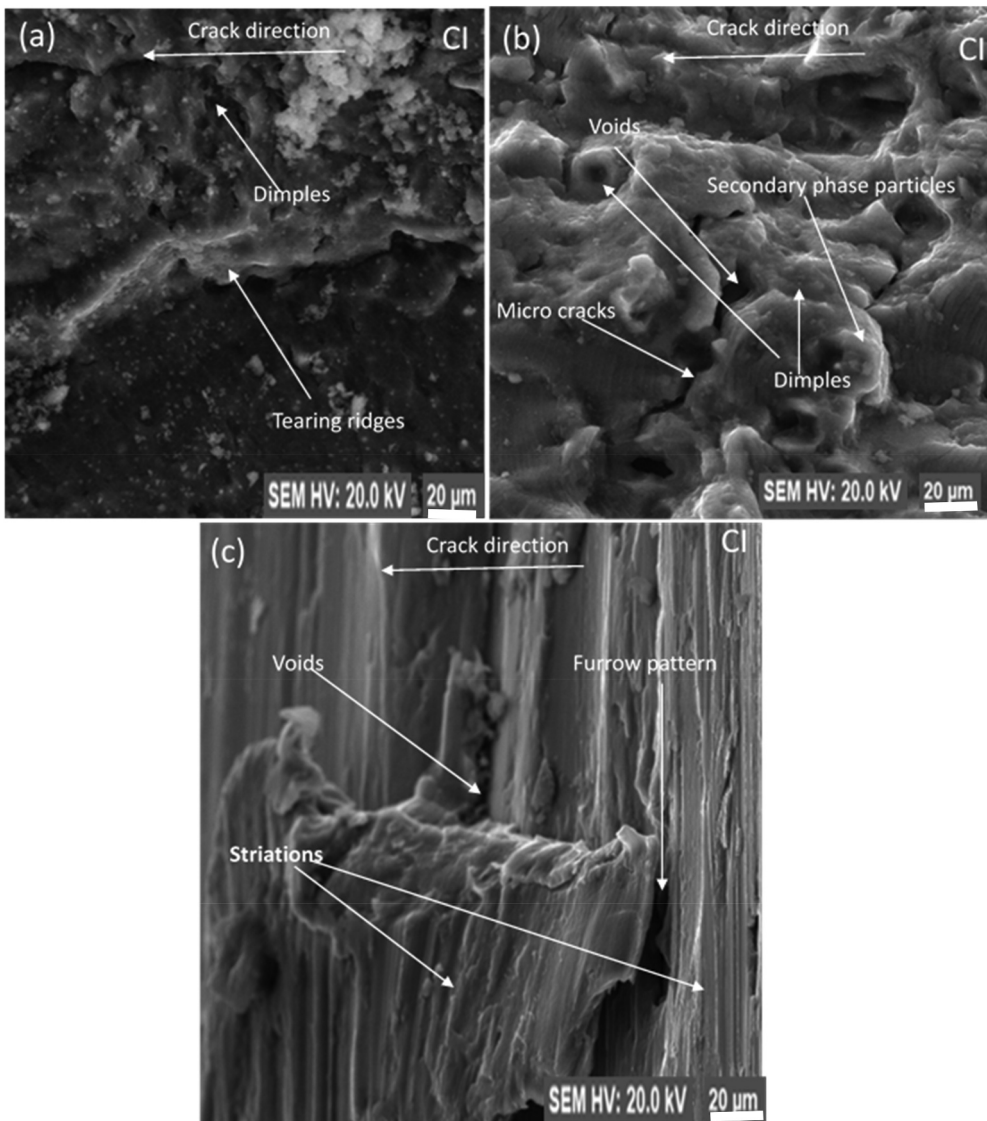

Figure 6. Fatigue-fractured surface morphology of the fatigue initiation of (a) Al alloy 7075-O, (b) Al alloy 7075-T6, (c) Al alloy 7075-T7.

The samples without internal tissue flaws, the stress concentration of the surface or subsurface commonly initiates fatigue cracks [23, 32, 33]. Internal tissue flaws include voids, inclusions, and uneven distribution of alloying elements or impurities within the material's microstructure. These imperfections are frequently tiny and cannot be noticeable to the human eye. They may be added during manufacturing or developed due to various situations during the formation of the material [31]. Other factors that lead to stress concentration flaws include minute porosity (tiny pores or voids caused by incomplete consolidation or trapped gases), surface scratches, and impurities developed when it is undergoing smelting and heat treatment. In these tests, the impurity phase particles separated from the matrix under the cyclic loading was where the crack was initiated. Chen *et al.* [34] and Clemens *et al.* [32] concluded that the impurity phase particles' Young's modulus, Poisson's ratio, and strength differ from those of the alloy matrix. Under cyclic loading, the impurity phase particles either fracture themselves or slide and detach from the rich iron phase matrix. The crucial zone's weakest point is where the crack first appears. The fatigue fracture is then formed as it spreads from the initiation to the inside along the path of perpendicular loading. The propagation rate is slow because the fatigue fracture initiation surfaces are exposed to the air [33]. When a metal is exposed to air, oxygen reacts with it to generate an oxide coating. This oxide layer can act as a stress concentrator and is brittle, which could cause the crack to spread. Second, a metal can rust if exposed to air [35]. Corrosion is the process by which chemicals eat away metal, which permits crack propagation. Temperature and humidity are other environmental factors that might affect the rate at which a fatigue crack spreads. High humidity can speed up corrosion, which can cause the crack to spread more quickly [34]. The fracture surface is made smooth and bright due to repeating open and close cyclic loading. Meanwhile, those cracks initiated at different planes meet during propagation; the radial stairs are left.
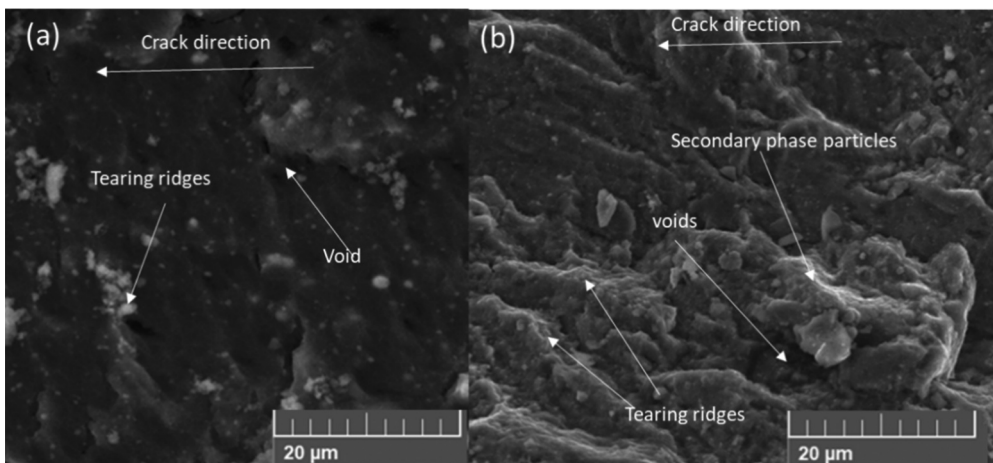

Figure 7. Fatigue crack propagation morphology of Al alloy 7075-O (a) CPS (b) CPF.

3.4.2. Fatigue crack propagation

The scanning electron microscopic morphology of fatigue crack propagation areas under a stress ratio of 0.33 and constant amplitude are shown in Figures 7, 8 and 9. The slow and fast crack propagation fractographic is depicted in the figures.

Figures 8(a) and 9(a) illustrate the initial fracture step due to fatigue propagation, which consists of two phases: crack initiation, followed by cracks propagating along the
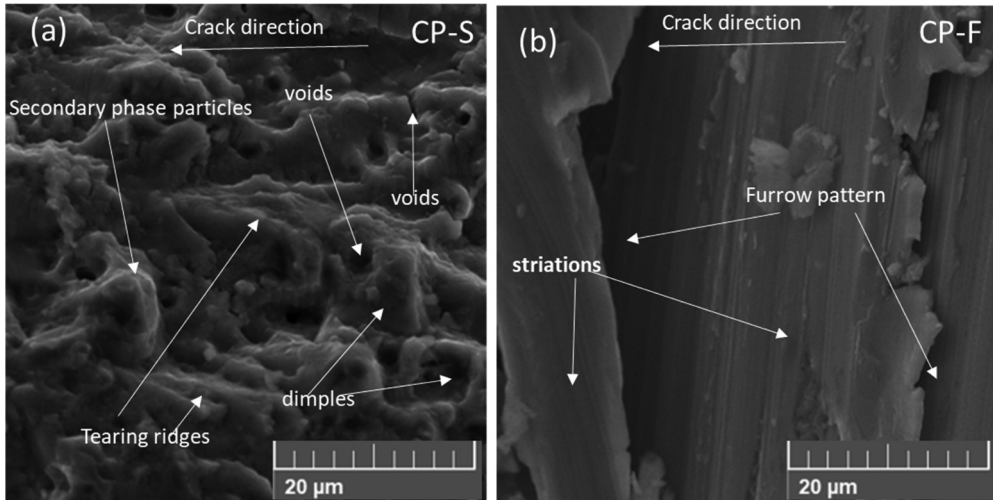

Figure 8. Fatigue crack propagation morphology of Al alloy 7075-T6, (a) slow crack propagation, (b) fast crack propagation.
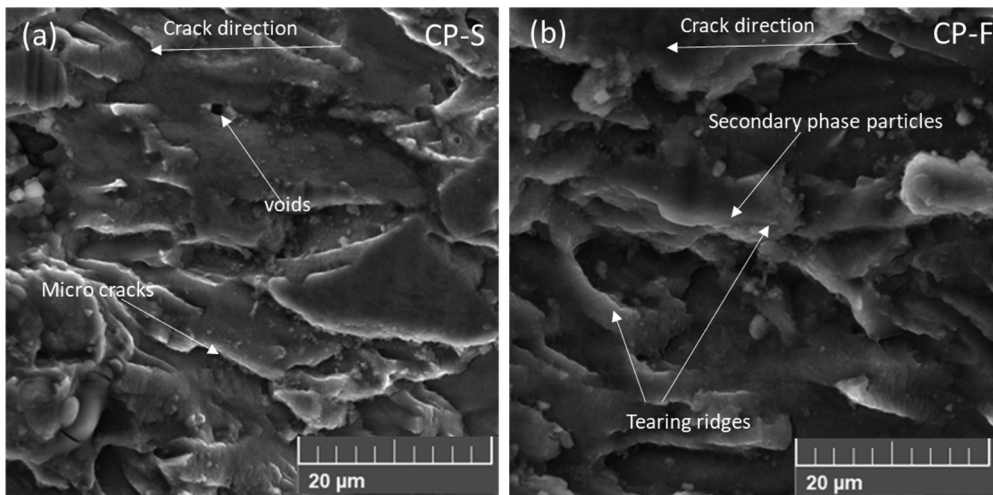

Figure 9. Fatigue crack propagation morphology of Al alloy 7075-T7, (a) slow crack propagation, (b) fast crack propagation.

primary slip plane of the slip band to the within of the material using the pure shear method. Figures 7(b), 8(b) and 9(b) show how the fatigue crack propagates for a particular length before changing directions and follows the stress' perpendicular orientation. These three phenomena are typical for the second phase of fatigue crack propagation. The quasi-cleavage fracture plane and the parallel zigzag area may be noticed on the fractography of aluminium alloy 7075, which has been aged at various Temper O, T6, and T7, as illustrated in Figures 8(a) and 9(a). After ageing treatment to different Temper O, T6 and T7, plenty of nano-strengthening phases leave in the matrix, the crack propagation is intercepted, and extensive deformation arises on the borders of cracks, leading to the cracks combining by ripping them and resulting in creating lamella fracture surface. The quasi-cleavage fracture plane's location of test Al alloy 7075–0 is the least, while the quasi-cleavage fracture plane's area of test Al alloy 7075-T7 is the most extensive. The form and extent of the quasi-cleavage fracture plane are linked with the alloy's micro-structure in the grain proportions state, the precipitated phase type, size, and disbandment, and the more extensive the grain, the bigger the quasi-cleavage fracture plane's area [36].

The second phase of the fatigue crack propagation displays fatigue strips. Individual strip denotes a stress cycle and indicates the crack tip site under this cycle, as is portrayed in Figures 7(b), 8(b) and 12(b). The average widths of tests Al alloys 7075-O, 7075-T6, and 7075-T7 are 0.28, 0.68 and 0.36 μm, respectively. Fatigue crack propagation surfaces exhibit some second micro-cracks parallel to the strips. The second stage particles thwart the crack propagation and alter the propagation direction; ultimately, the crack continues propagating after going around them.

When subjected to cyclic loading, the holes are left because of the second-stage particles desquamating from the matrix. By measuring the size of the holes, the diameter of the second stage particles is 2–3 μm, adversely impacting high cycle fatigue performance. In addition, numerous nanoscale precipitated stage particles are distributed in the matrix, favouring high cycle fatigue performance.

3.4.3. Final fracture

The final fatigue-fractured surface morphology of Al alloy (a) 7075-O, (b) 7075-T6, and (c) 7075-T7 is outlined in Figure 10.

The material cannot handle the cyclic loading when the crack length comes to the critical length. Unstable crack propagation is experienced, eventually leading to transient material fracture. Final fracture SEM images are displayed in Figure 10 for Al alloy (a) 7075-O, (b) 7075-T6, and (c) 7075-T7. The surfaces of the final fracture are coarse and mixed ductile-brittle fractures with numerous tearing ridges, as noticed in Figure 10(a–c). The dimple size measured through the SEM machine for Al alloy 7075-O is the smallest (11 μm), and the size is the most diminutive. The outcomes indicate that the dimple dimensions and depth of Al alloy 7075 gain slowly with the increase of heat treatment from 11 μm in 7075-O to 15 μm in 7075-T6 to 18 μm in 7075-T7. The number of dimples is closely
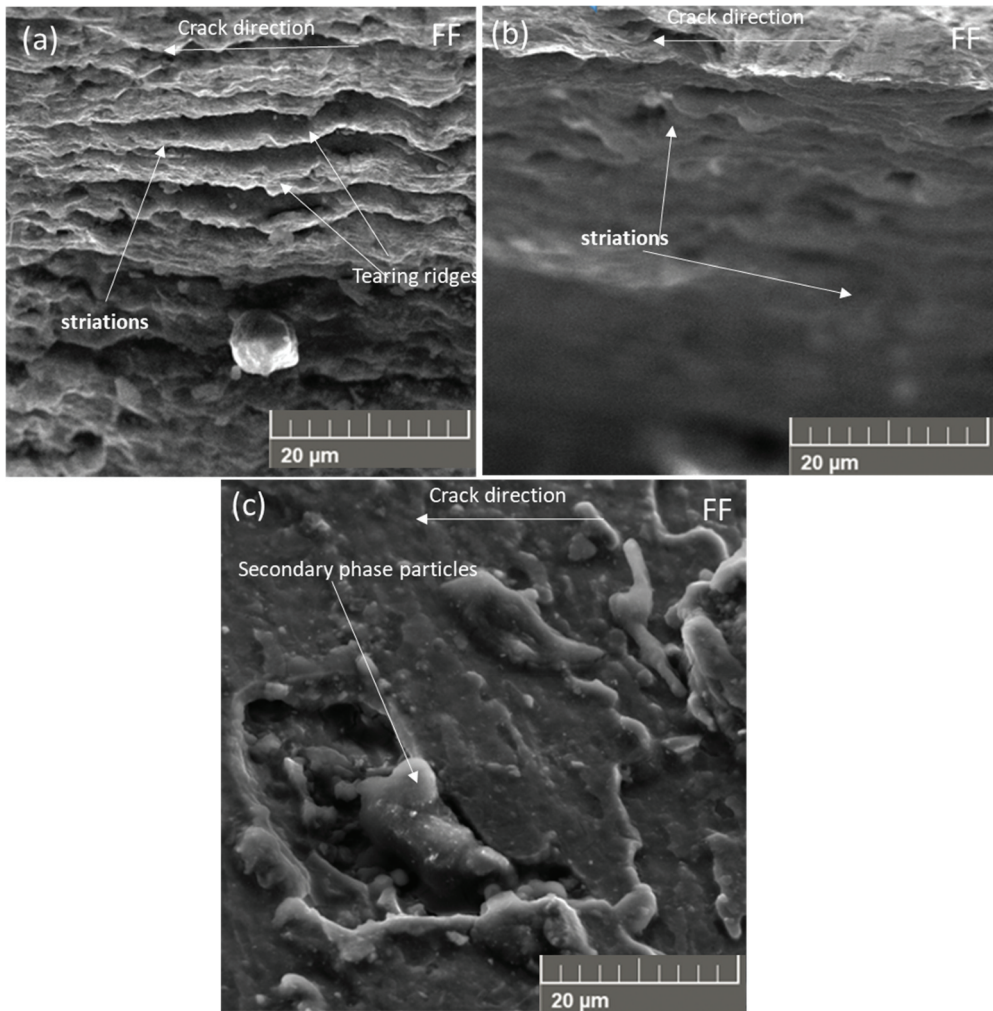
Figure 10. Final fatigue-fractured surface morphology of (a) Al alloy 7075-O, (b) Al alloy 7075-T6, (c) Al alloy 7075-T7.

associated with the precipitated stage particles. The better and the finer precipitated stage particles, the more the dimples. It can be therefore inferred that the more Al alloy 7075 is heat-treated, the more finely predicated phase particles occur.

3.5. Fractographic analysis of different hole orientations

3.5.1. Fatigue crack initiation to study hole geometry
Figures 11 and 12 show SEM sections for crack initiation for different hole geometries and varied heat treatment conditions. Fracture surfaces were examined with an
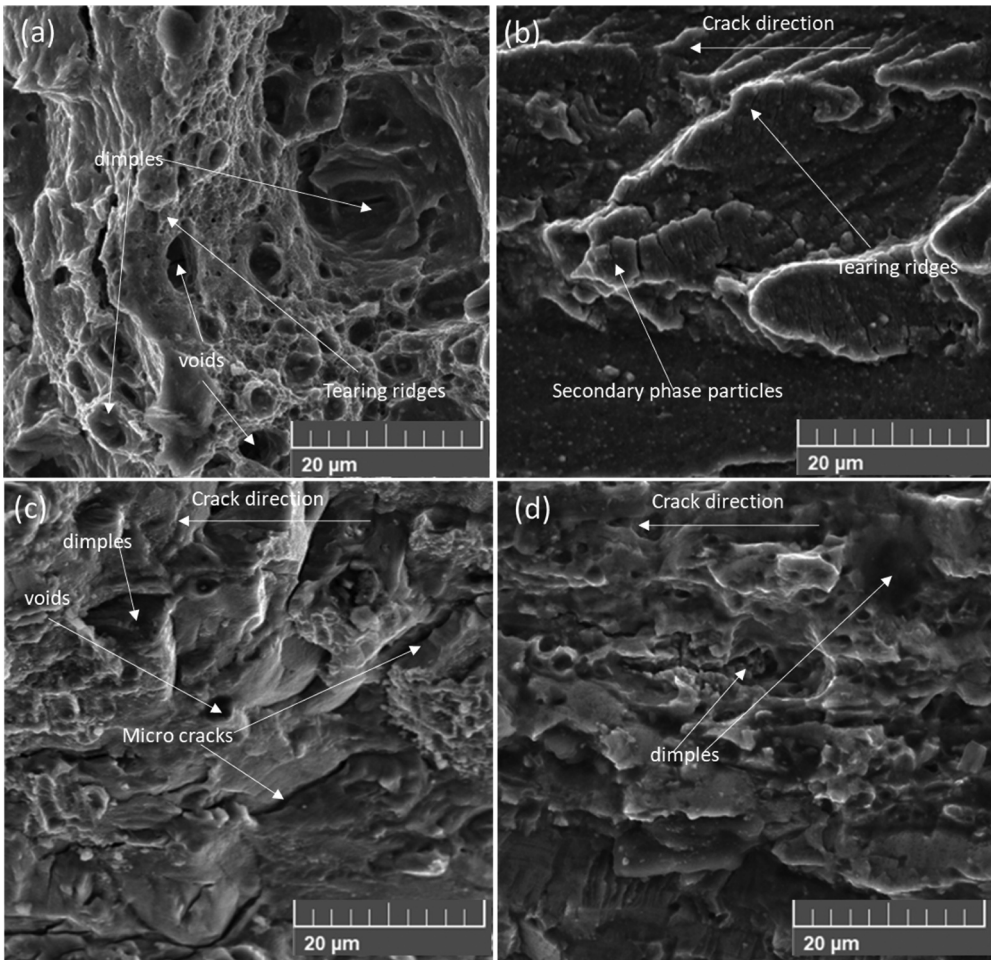
Figure 11. Fatigue crack initiation morphology of (a) Al alloy 7075-O countersunk rivet hole, (b) Al alloy 7075-O perpendicular rivet hole, (c) Al alloy 7075-T6 countersunk rivet hole, (d) Al alloy 7075-T6 perpendicular rivet hole.

SEM. The statistics show crystallographic facets characterising stage I growth on specimens tested in air.

Fatigue cracking starts at the countersink for a chamfered hole (after initiation on the other side, a crack is noticed propagating along the countersink after initiation on the opposite side in all cases). Nevertheless, crack initiation is consistently trans-granular, despite the existence of some crystallographic facets that are anticipated during stage I growth. Under the fracture surface exist micro-cracks connecting pits together [37]. Micro-cracks starting from the cladding and/or at the cladding/core metal interface are also noticed in both straight hole and chamfer hole samples.
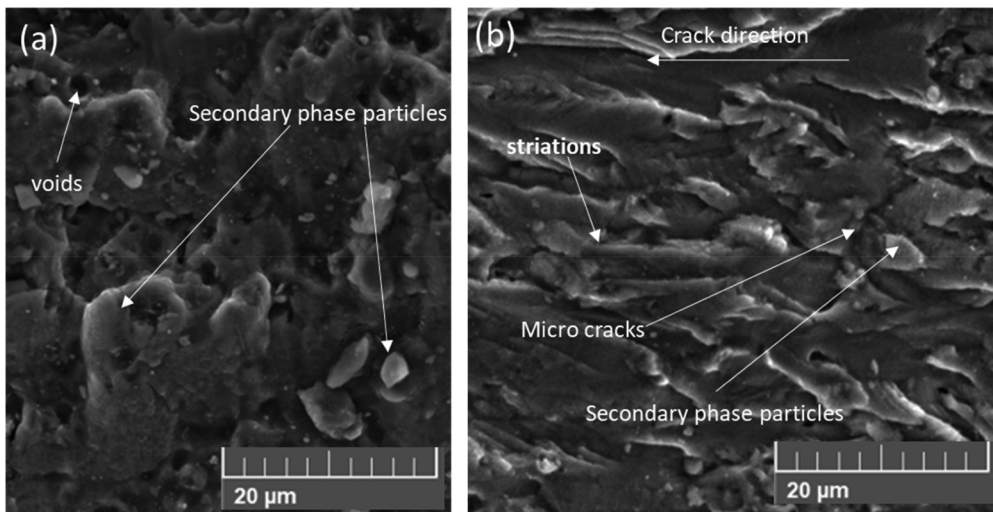
Figure 12. Fatigue crack initiation morphology of Al alloy 7075-T7, (a) countersunk rivet hole, (b) perpendicular rivet hole.

3.5.2. Fatigue crack propagation to study hole geometry

The SEM results on fast and slow crack propagation at different rivet hole orientations and varied heat treatments are shown in Figures 13,14, and 15.

A significant disparity was noticed in fractographic attributes between the Al alloy 7075-O, 7075-T6, and 7075-T7 conditions and an insignificant difference between the countersunk and perpendicular rivet hole geometry. The typical fractographs of the Al alloy 7075-O, 7075-T6, and 7075-T7 specimens of stress ratios 0.33 are shown for two different rivet hole geometry (countersunk and perpendicular). Slow fatigue crack propagation growth rate images for the different rivet hole orientations are shown in Figures 13(b), 14(a), 14(c), 15(a), and 15 (c). In contrast, images for fast crack propagation growth rates for different rivet hole orientations are shown in Figures 13(a–c), 14(b–d), 14(d), 15(b–d). Countersunk rivet holes establish a smooth surface on the structure by allowing flush placement of rivet heads. Stress concentration is the crucial factor that countersunk rivet holes affect when it comes to fatigue fracture initiation. When a hole is countersunk, the area surrounding the hole's edge thins out, causing tension to concentrate there. Compared to the rest of the structure, that location may experience higher stress levels due to stress concentration. As a result, under cyclic loads, fatigue cracks are more prone to start at or close to the countersink zone. Conventional holes without any countersinking or tapering are drilled through the centre of the material to form perpendicular rivet holes. The load distribution surrounding the hole is primarily responsible for how perpendicular rivet holes affect the development of fatigue cracks. As there are no stress concentration spots at the hole's borders, the stress
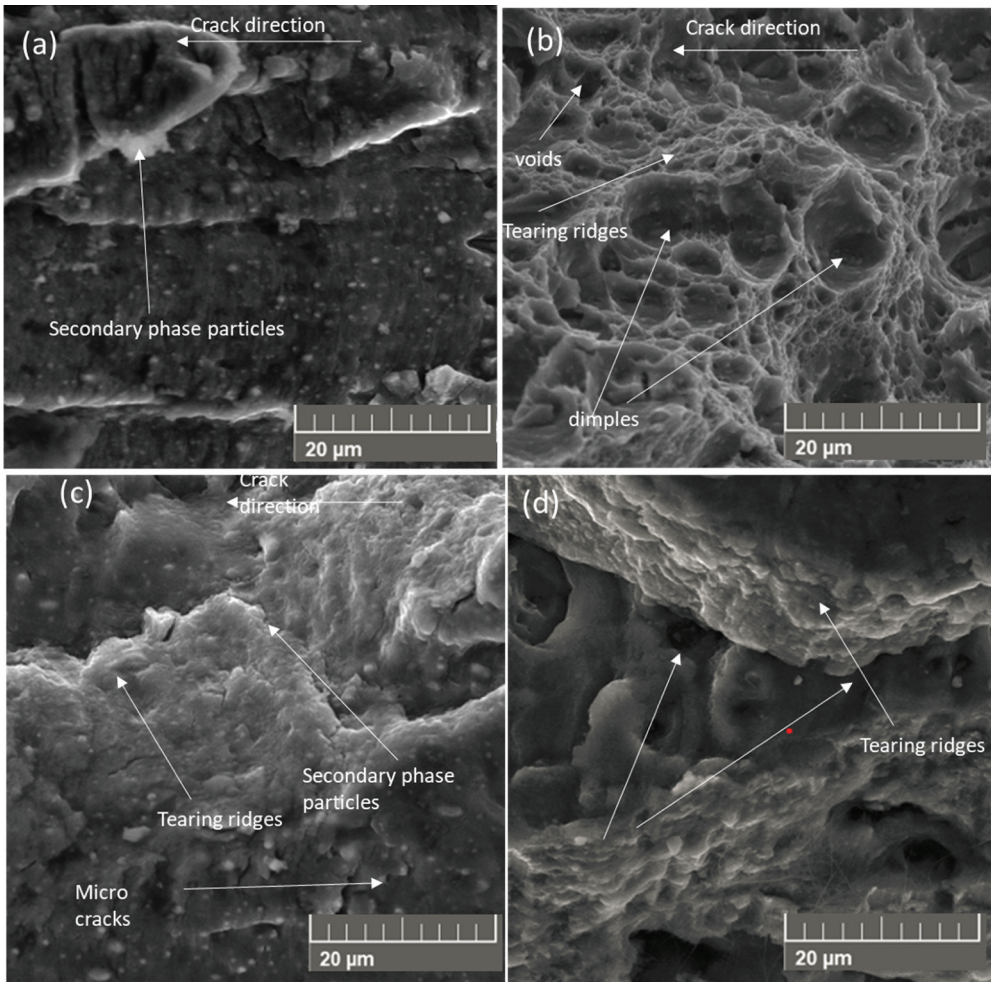
Figure 13. Fatigue crack propagation morphology of Al alloy 7075-O, (a) CPS- countersunk rivet hole, (b) CPF- countersunk rivet hole, (c) CPS- perpendicular rivet hole, (d) CPF - perpendicular rivet hole.

distribution in this instance is considerably more uniform than in countersunk holes. However, due to stress concentrations that may develop at the hole's edge, perpendicular rivet holes can still contribute to the development of a fatigue crack. Additionally, improper hole alignment or excessive rivet tightening might create residual stresses that could encourage the start of a fatigue crack [35].

An increase in ΔK makes crack propagation entirely trans-granular. There is clear visibility of beach marks. A constituent particle is at the base of a dimple. A faceted fatigue crack growth depicts the Al alloy 7075-O state. The facets are constituted on crystallographic planes, their direction shifts from grain to grain, and the crack surface is relatively rough. They are compatible with an essentially planar slip mode, which
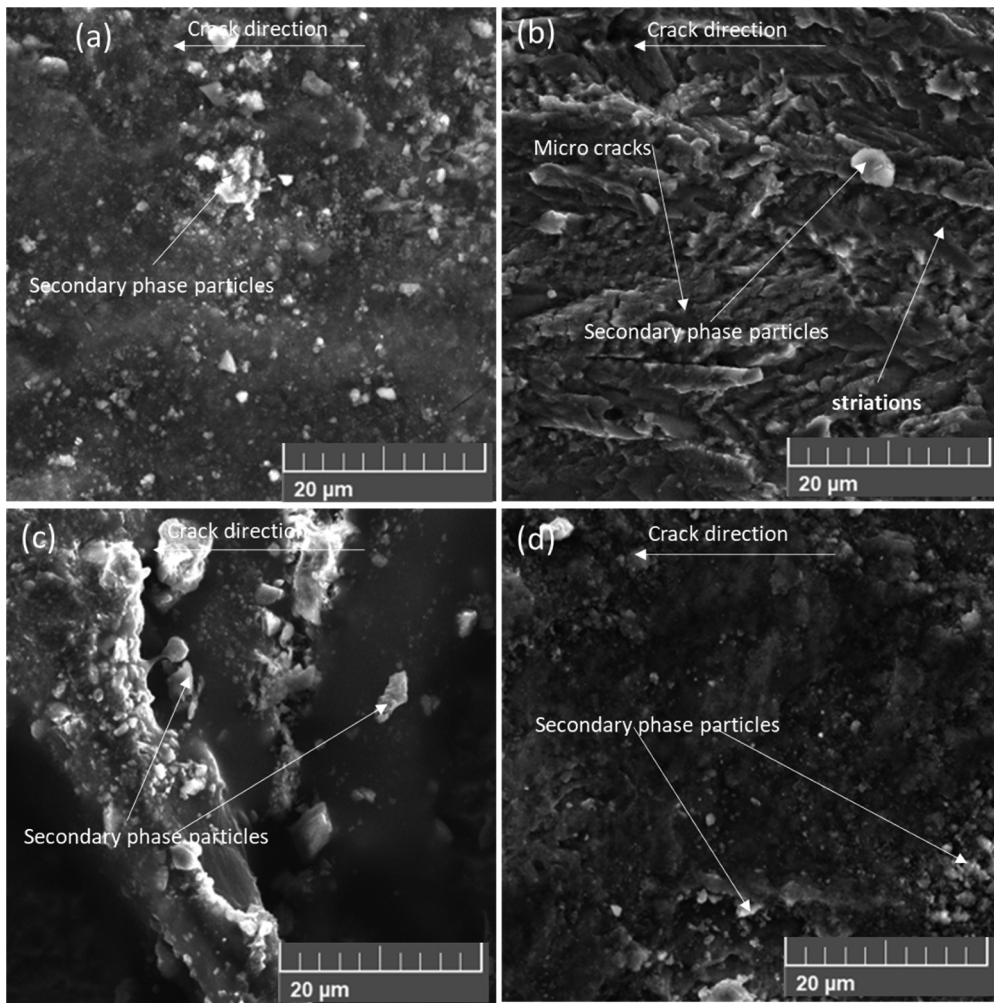
Figure 14. Fatigue crack propagation morphology of Al alloy 7075-T6, (a) CPS – countersunk rivet hole, (b) CPF – countersunk rivet hole, (c) CPS – perpendicular rivet hole, (d) CPF – perpendicular rivet hole.

happens when the precipitates are shearable [38]. The crack surface of the Al alloy 7075-T7 sample is relatively flat, displaying some regions without features, patches of faint striations, and dimples.

3.5.3. Final fracture to study hole geometry

The SEM results on final crack fracture at different rivet hole orientations and varied heat treatments are shown in Figures 16 and 17.

A substantial contrast is visible in fractographic characteristics between the Al alloy 7075-O, 7075-T6, and 7075-T7 conditions and an insignificant difference
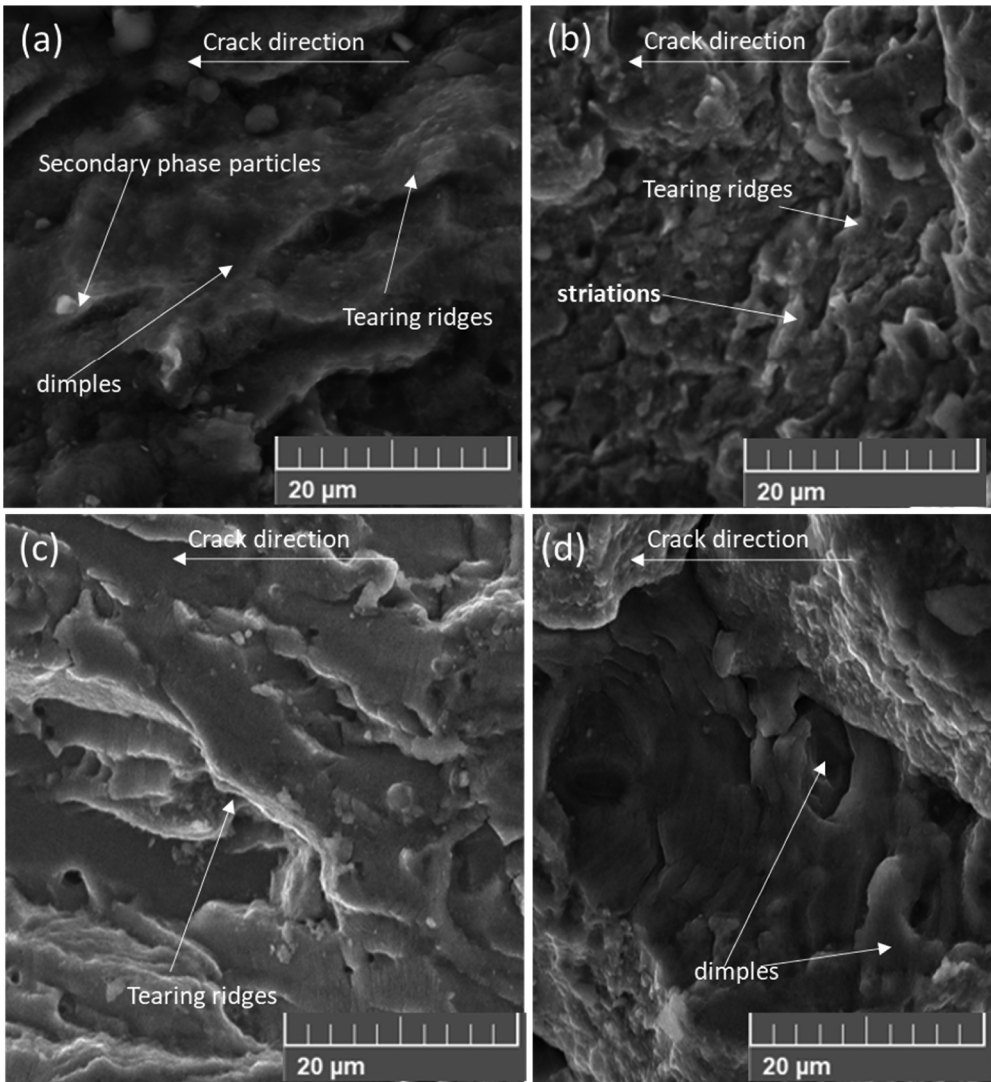
Figure 15. Fatigue crack propagation morphology of Al alloy 7075-T7, (a) CPS – countersunk rivet hole, (b) CPF – countersunk rivet hole, (c) CPS – perpendicular rivet hole, (d) CPF – perpendicular rivet hole.

between the countersunk and perpendicular rivet hole geometry for the same temper condition. The typical fractographs of the Al alloy 7075-O, 7075-T6, and 7075-T7 specimens of stress ratios 0.33 are shown for two different rivet hole geometry (countersunk and perpendicular). Figures 16 and 17 show SEM views for crack initiation, slow and fast crack propagation, and final fatigue fracture. A faceted fatigue crack growth depicts the Al alloy 7075-O state. The facets are
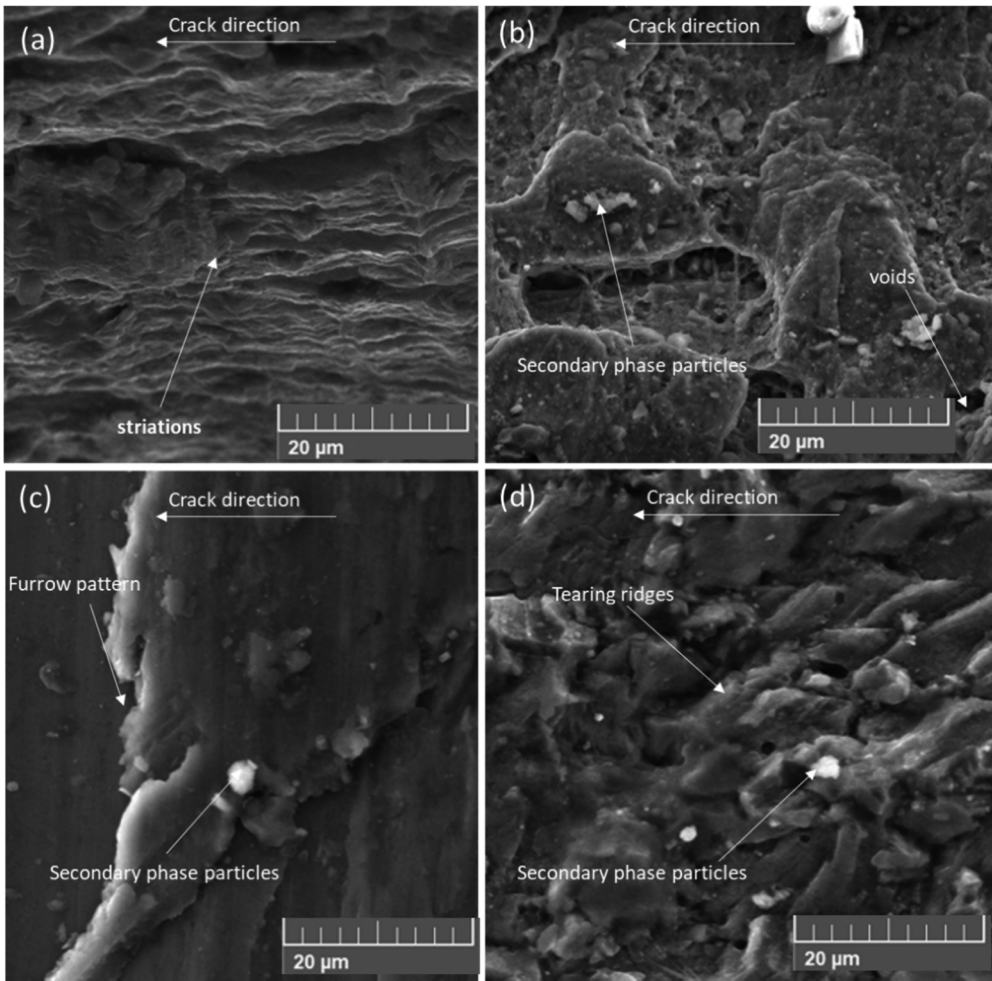
Figure 16. Final fatigue fracture morphology of Al alloy, (a) 7075-O countersunk rivet hole, (b) 7075-O perpendicular rivet hole, (c) 7075-T6 countersunk rivet hole, (d) 7075-T6 perpendicular rivet hole.

constituted on crystallographic planes, their direction transitions from grain to grain, and the crack surface is relatively rough. They agree with a predominantly planar slip mode, which transpires when the precipitates are shearable [39–41]. The crack surface of the Al alloy 7075-T7 sample is somewhat flat, showing some regions without features, patches of murky striations, and dimples. Like other aluminium alloys, the present results on metallurgy Al alloy 7075 demonstrate that Al alloy 7075-T7 micro-structures have prominent near-threshold fatigue crack propagation resistance to Al alloy 7075-T6 and Al alloy 7075-O micro-structures.
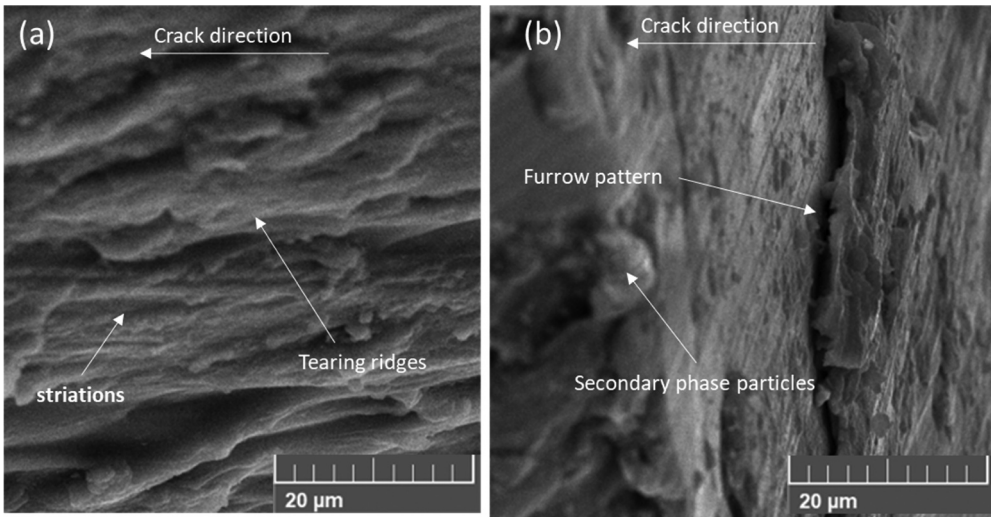
Figure 17. Final fatigue fracture morphology of Al alloy 7075-T7, (a) countersunk rivet hole, (b) perpendicular rivet hole.

4. Conclusion

This study found that The Al 7075-T7 yielded greater resistance to threshold fatigue crack growth, shown by greater ΔK & and K_{max}, than the Al 7075-O and T6. It was noticed that fatigue strength varied depending on the specimen's heat treatment. With increasing ageing from O to T6 to T7, the fatigue performances increase, and the fatigue curves of Al-7075 T6 are close to that of Al-7075 T7. As expected, crack orientation did not affect the cracking of Al 7075. The 7075-aluminium alloy under the temper O showed the same fatigue performances for specimens designed with countersunk and perpendicular rivet hole orientation. The ageing treatment improves fatigue performance for the same rivet hole orientations. With increasing ageing conditions (aged at O, T6, T7) for the same rivet hole orientation (100° countersunk or perpendicular), the fatigue performances increase from O to T6 to T7.

Resistance to fatigue crack elongation increases with an increase in heat treatment from -O to -T6 to -T7 showing growth rate at the near-threshold being slower and fatigue threshold ΔK_{th} values higher, agreeing with decreased measured levels of crack closure and a diminishing crack path tortuosity. It was evident in fatigue fractured surface SEM reviews that micro-cracks that induce fracturing initiate from zones where inclusions, coarse, secondary stage grains, and micro-structural flaws are present or in the regions very near to these areas and cause fatigue fracture. The Al 7075-O state exhibited a micro-structure possessing coherent, shearable precipitates and a tortuous and faceted crack path. Meanwhile, the Al 7075-T7 and Al 7075-T6 showed micro-structure comprising incoherent and non-shearable precipitates and an almost straight crack path. The coherent shearable precipitates resulted in a more significant threshold fatigue crack growth resistance of the Al 7075-O specimen. Those precipitates promote reversible planar slip, facilitate crack deflection and branching, decrease the effective stress intensity factor for fatigue crack growth, and delay fatigue crack growth.

Some structural designs allow fatigue cracks to happen after an acceptable lifetime, but they should have a low risk of an entire failure. The crack initiation life is similarly of interest, and it should be extensive enough for an acceptable in-service lifetime. If failure is inappropriate, a dependable inspection technique is necessary. This is used in aircraft structures and can be applied to several structural joints. As an outcome, both the crack initiation life and the crack growth life are essential.

Disclosure statement

No potential conflict of interest was reported by the author(s).

ORCID

Shagwira Harrison ⓘ http://orcid.org/0000-0002-1115-932X

References

[1] Lin R, Liu B, Zhang J, et al. Microstructure evolution and properties of 7075 aluminum alloy recycled from scrap aircraft aluminum alloys. J Mater Res Technol. 2022;19(3):354–367. doi: 10.1016/j.jmrt.2022.05.011
[2] Gloria A, Montanari R, Richetta M, et al. Alloys for aeronautic applications: state of the art and perspectives. Metals. 2019;9(6):662. doi: 10.3390/met9060662
[3] Younis HB, Kamal K, Sheikh MF, et al. Prediction of fatigue crack growth rate in aircraft aluminum alloys using optimized neural networks. Theor Appl Fract Mech. 2022;117 (3):103196. doi: 10.1016/j.tafmec.2021.103196
[4] Boyer RR, Cotton JD, Mohaghegh M, et al. Materials considerations for aerospace applications. MRS Bull. 2015;40(12):1055–1066. doi: 10.1557/mrs.2015.278
[5] Rambabu P, Eswara Prasad N, Kutumbarao VV, et al. Aluminium alloys for aerospace applications. In: Prasad NE Wanhill RJH, editors Indian Institute of Metals Series, Aerospace Materials and Material Technologies. Singapore: Springer Singapore; 2017. pp. 29–52.
[6] T. B. C. MOM-MOM-19-0536-01B. Information - 737NG STA 663.75 FRAME FITTING and FAILSAFE STRAP CRACKS at S-18A STRAP. Oct 2019.
[7] Dursun T, Soutis C. Recent developments in advanced aircraft aluminium alloys. Mater Design. 2014;56:862–871. doi: 10.1016/j.matdes.2013.12.002
[8] Benachour, Benguediab M. Fatigue crack initiation of Al-alloys "Effect of heat treatment condition". 2013. doi: 10.5281/zenodo.1089036
[9] Khodabakhshi AR, Khodabakhshi M. Effects of non-isothermal annealing on microstructure and mechanical properties of severely deformed aluminum samples: modeling and experiment. Trans Nonferrous Met Soc China. 2019;29(6):1127–1137. doi: 10.1016/S1003-6326(19)65021-1
[10] Huang B, Kaynak Y, Arvin C, et al. Improved surface integrity from cryogenic machining of Al 7050-T7451 alloy with ultrafine-grained structure. Adv Mater Process Technol. 2015;1 (3–4):3-4, pp. 361–374. doi: 10.1080/2374068X.2015.1127543
[11] Fakioglu A, Özyürek D, Yilmaz R. Effects of different heat treatment conditions on fatigue behavior of AA7075 alloy. High Temp Mater Process. 2013;32(4):345–351. doi: 10.1515/htmp-2012-0146
[12] Gačo D, Hrnjica B, Bajramović E, Toughness and fatigue analysis of al 6xxx alloys. 2017.

[13] Lee MH, Fatigue life, fatigue crack propagation and fracture toughness study of 7075 aluminum alloy subjected to thermomechanical processing. 1984.

[14] Zaiken E, Ritchie RO. Effects of microstructure on fatigue crack propagation and crack closure behavior in aluminum alloy 7150. Mater Sci Eng. 1985;70:151–160. doi: 10.1016/0025-5416(85)90276-9

[15] Sajadifar SV, Krooß P, Fröck H, et al. Effects of aging under stress on mechanical properties and microstructure of EN AW 7075 alloy. Metals. 2021;11(7):1142. doi: 10.3390/met11071142

[16] Borrego LP, Costa JM, Antunes FV, et al. Fatigue crack growth in heat-treated aluminium alloys. Eng Fail Anal. 2010;17(1):11–18. doi: 10.1016/j.engfailanal.2008.11.007

[17] Zupanič F, Klemenc J, Steinacher M, et al. Microstructure, mechanical properties and fatigue behaviour of a new high-strength aluminium alloy AA 6086. J Alloys Compd. 2023;941:168976. doi: 10.1016/j.jallcom.2023.168976

[18] Cheraghi SH. Effect of variations in the riveting process on the quality of riveted joints. Int J Adv Manuf Technol. 2008;39(11–12):11-12, pp. 1144–1155. doi: 10.1007/s00170-007-1291-6

[19] Pandiyarajan R, Arumugam K, Prabakaran MP, et al. Fatigue life and fatigue crack growth rate analysis of high strength low alloy steel (42CrMo4). Mater Today Proc. 2021;37 (5):1957–1962. doi: 10.1016/j.matpr.2020.07.486

[20] Test Method for Measurement of Fatigue Crack Growth Rates, E08 committee. West Conshohocken, PA: ASTM International; 2011. doi: 10.1520/e1820-11

[21] Hörnqvist M, Hansson T, Clevfors O. Fatigue crack growth testing using varying ratios. Procedia Eng. 2010;2(1):155–161. doi:10.1016/j.proeng.2010.03.017

[22] Yao L, Chuai M, Liu J, et al. Fatigue delamination behavior in composite laminates at different stress ratios and temperatures. Int J Fatigue. 2023;175:107830. doi: 10.1016/j.ijfatigue.2023.107830

[23] Yusuf BO, Mamrung YPC, Welded high strength low alloy steel influence on fatigue crack propagation using LEFM: a practical and thematic review.

[24] Duchaczek A, Mańko Z. Determination of the value of stress intensity factor in fatigue life of steel military bridges. Eur J Environ Civ Eng. 2015;19(8):1015–1032. doi: 10.1080/19648189.2014.992549

[25] Murakami Y. Effect of size and geometry of small defects on the fatigue limit. In: Metal Fatigue. Elsevier; 2019. pp. 39–59.

[26] Burzić Z, Sedmak A, Sedmak S, et al. Analysis of fatigue behaviour of a bridge welded structure. Procedia Struct Integr. 2022;37(1):269–273. doi: 10.1016/j.prostr.2022.01.084

[27] Reimann WH, Brisbane AW. Improved fracture resistance of 7075 through thermomechanical processing. Eng Fract Mech. 1973;5(1):67–78. doi: 10.1016/0013-7944(73)90008-8

[28] Main B, Jones M, Dixon B, et al. On small fatigue crack growth rates in AA7085-T7452. Int J Fatigue. 2022;156(7):106704. doi: 10.1016/j.ijfatigue.2021.106704

[29] Bucci RJ. Selecting aluminum alloys to resist failure by fracture mechanisms. Eng Fract Mech. 1979;12(3):407–441. doi: 10.1016/0013-7944(79)90053-5

[30] Aamir M, Giasin K, Tolouei-Rad M, et al. A review: drilling performance and hole quality of aluminium alloys for aerospace applications. J Mater Res Technol. 2020;9(6):12484–12500. doi: 10.1016/j.jmrt.2020.09.003

[31] Dæhli LEB, Olufsen SN, Kristensen TA, et al. Influence of constituent particles on fracture of aluminium alloys under high-triaxiality loading. Mater Sci Eng A. 2023;864(11):144531. doi: 10.1016/j.msea.2022.144531

[32] Clemens H, Mayer S, Scheu C. Microstructure and properties of Engineering materials. In: Staron P, Schreyer A, Clemens H Mayer S, editors. Neutrons and synchrotron radiation in engineering materials science. Weinheim, Germany: Wiley-VCH Verlag GmbH & Co. KGaA; 2017. pp. 1–20. doi: 10.1002/9783527684489.ch1

[33] Lu D, Lin B, Liu T, et al. Effect of grain structure on fatigue crack propagation behavior of Al-cu-li alloys. J Mater Sci Technol. 2023;148:75–89. doi: 10.1016/j.jmst.2022.10.085

[34] Pereira GS, Cavalcante TRF, Cid MC, et al. Effect of saline environment on the fatigue crack growth resistance of WE43 mg alloy. Mater Today Commun. 2022;31:103788. doi: 10.1016/j.mtcomm.2022.103788

[35] Lal Dhaker K, Bhilala K, Kishor Sharma H, et al. Experimental investigation of hole geometry during electric discharge drilling of aerospace material sheet. Mater Today Proc. 2023;78(2):570–579. doi: 10.1016/j.matpr.2022.11.471

[36] Yang D, Liu Y, Li S, et al. Effects of aging temperature on microstructure and high cycle fatigue performance of 7075 aluminum alloy. J Wuhan Univ Technol Mat Sci Edit. 2017;32 (3):677–684. doi:10.1007/s11595-017-1652-4

[37] Kedir YA, Lemu HG. Prediction of fatigue crack initiation under variable amplitude loading: literature review. Metals. 2023;13(3):487. doi: 10.3390/met13030487

[38] Wu Y, Wang J, Shao C, et al. Insights into the effects of δ-ferrite on crack tip stress/strain and stress corrosion cracking propagation behavior of austenite weld metal: a numerical and experimental study. Int J Pres Ves Pip. 2023;205(1):105007. doi: 10.1016/j.ijpvp.2023.105007

[39] Leng L, Zhang ZJ, Duan QQ, et al. Improving the fatigue strength of 7075 alloy through aging. Mater Sci Eng A. 2018;738:24–30. doi: 10.1016/j.msea.2018.09.047

[40] Chen S-Y, Chen K-H, Dong P-X, et al. Effect of heat treatment on stress corrosion cracking, fracture toughness and strength of 7085 aluminum alloy. Trans Nonferrous Met Soc China. 2014;24(7):2320–2325. doi: 10.1016/S1003-6326(14)63351-3

[41] De P, Mishra R, Smith C. Effect of microstructure on fatigue life and fracture morphology in an aluminum alloy. Scripta Materialia. 2009;60(7):500–503. doi: 10.1016/j.scriptamat.2008.11.032